

Semi-Smooth Newton Algorithm for Non-Convex Penalized Linear Regression

Yueyong Shi, Jian Huang, Yuling Jiao, and Qinglong Yang

Abstract—Both the smoothly clipped absolute deviation (SCAD) and the minimax concave penalty (MCP) penalized linear regression models are capable of dealing with variable selection and parameter estimation simultaneously. Theoretically, these two models enjoy the oracle property even in the high dimensional settings where the number of predictors p may be much larger than the number of observations n . However, numerically, it is quite challenging to develop fast and stable algorithms due to their non-convexity and non-smoothness. In this paper we develop a fast algorithm for SCAD and MCP penalized problems. First, we derive that the global minimizers of both models are roots of some nonsmooth equations. Then, Semi-smooth Newton (SSN) algorithm is employed to solve the equations. We prove the local superlinear convergence of SSN algorithm. Computational complexity analysis demonstrates that the cost of SSN algorithm per iteration is $O(np)$. Combining with the warmstarting technique SSN algorithm can be very efficient. Simulation studies and real data examples show that SSN algorithm greatly outperforms coordinate descent in computational efficiency while reaching comparable accuracy.

Index Terms—Convergence, MCP, SCAD, Semi-smooth Newton algorithm, Warmstarting.

I. INTRODUCTION

THIS paper introduces a fast algorithm for concavely penalized regression. We focus on the linear regression model

$$y = X\beta^\dagger + \varepsilon, \quad (1)$$

where $y \in \mathbb{R}^n$ is an $n \times 1$ vector of response variables, $X = (X_1, \dots, X_p)$ is an $n \times p$ design matrix, ε is an $n \times 1$ vector of error terms, and $\beta^\dagger = (\beta_1^\dagger, \dots, \beta_p^\dagger)^T \in \mathbb{R}^p$ is the underlying regression coefficient vector.

Under the sparsity assumption that the number of important predictors is relatively small, it is natural to consider the

The work of Y. Shi was supported by the National Natural Science Foundation of China under Grant 11501578, Grant 11701571, Grant 11801531 and Grant 41572315. The work of Y. Jiao was supported in part by the National Science Foundation of China under Grant 11501579 and Grant 11871474, and in part by the Natural Science Foundation of Hubei Province under Grant 2016CFB486. The work of Q. Yang was supported by the National Science Foundation of China under Grant 11671311. (Corresponding author: Qinglong Yang.)

Y. Shi is with the School of Economics and Management, China University of Geosciences and Center for Resources and Environmental Economic Research, China University of Geosciences, Wuhan 430074, China (e-mail: syywd@whu.edu.cn).

J. Huang was with the Department of Applied Mathematics, The Hong Kong Polytechnic University, Hong Kong 999077, China (e-mail: j.huang@polyu.edu.hk).

Y. Jiao and Q. Yang are with the School of Statistics and Mathematics, Zhongnan University of Economics and Law, Wuhan 430073, China (e-mails: yulingjiaomath@whu.edu.cn; qinglongyang.stat@gmail.com).

estimator that solves the minimization problem:

$$\min_{\beta \in \mathbb{R}^p} \|X\beta - y\|_2^2, \quad \text{subject to } \|\beta\|_0 \leq \tau, \quad (2)$$

where $\|\beta\|_0$ denotes the number of nonzero elements of β and $\tau > 0$ is a tuning parameter controlling the sparsity level. However, the minimization problem (2) is NP-hard [1], hence it is quite challenging to design a feasible algorithm for solving it when p is large. Replacing the $\|\beta\|_0$ term in (2) by $\|\beta\|_1$, we get the ℓ_1 penalized problem or the LASSO [2]

$$\min_{\beta \in \mathbb{R}^p} \|X\beta - y\|_2^2, \quad \text{subject to } \|\beta\|_1 \leq \tau. \quad (3)$$

which can be viewed as a convex relaxation of (2). Numerically, it is convenient to consider the Lagrange form of (3):

$$\min_{\beta \in \mathbb{R}^p} \frac{1}{2} \|X\beta - y\|_2^2 + \lambda \|\beta\|_1. \quad (4)$$

This is known as the basis pursuit denoising (BPDN) in the signal processing literature [3]. Computationally, (4) is a convex minimization problem, therefore, several fast algorithms have been proposed for computing its global minimizer, such as Homotopy or LARS [4], [5] and coordinate descent (CD) algorithm [6], [7], [8].

Theoretically, under certain regularity conditions on the design matrix X , such as restricted isometry property [9], strong irrepresentable condition [10], [11] and sparsity condition on the regression coefficients, LASSO has attractive estimation and selection properties. However, even under these conditions, the minimizer of (4) still suffers from the so-called LASSO bias, which implies that the LASSO regularized estimator does not have the oracle property. To remedy this problem, [12] proposed using concave penalties that can reduce bias and still yield sparse solutions. This leads to the following minimization problem

$$\min_{\beta \in \mathbb{R}^p} \frac{1}{2} \|X\beta - y\|_2^2 + \sum_{i=1}^p p(\beta_i; \lambda, \gamma), \quad (5)$$

where $p(\cdot; \lambda, \gamma)$ is a concave function with penalty parameter λ and γ is a given parameter that controls the concavity of p . We will focus on the smoothly clipped absolute deviation (SCAD) penalty [12] and the minimax concave penalty (MCP) [13].

The SCAD penalty is

$$p_{scad}(t; \lambda, \gamma) = \lambda \int_0^t \min\{1, (\gamma - x/\lambda)_+ / (\gamma - 1)\} dx, \quad \gamma > 2, \quad (6)$$

and the MCP takes the form

$$p_{mcp}(t; \lambda, \gamma) = \lambda \int_0^t (1 - x/(\gamma\lambda))_+ dx, \gamma > 1, \quad (7)$$

where γ is a parameter that controls the concavity of the penalty function and x_+ is the nonnegative part of x , i.e., $x_+ = x1_{\{x \geq 0\}}$. In particular, both penalties converge to the ℓ_1 penalty as $\gamma \rightarrow \infty$, and the MCP converges to the hard-thresholding penalty as $\gamma \rightarrow 1$. The MCP can be easily understood by considering its derivative,

$$\dot{p}_{mcp}(t; \lambda, \gamma) = \lambda(1 - |t|/(\gamma\lambda))_+ \text{sign}(t), \quad (8)$$

where $\text{sign}(t) = -1, 0$, or 1 if $t < 0, = 0$, or > 0 . The MCP provides a continuum of penalties with the ℓ_1 penalty at $\gamma = \infty$ and a continuous approximation of the hard-thresholding penalty as $\gamma \rightarrow 1$.

Concavely penalized estimators have the asymptotic oracle property under appropriate conditions [12], [13]. However, it is quite challenging to solve (5) with (6) and (7) numerically, since the objective functions to be minimized are both non-convex and nonsmooth. Several methods have been proposed to deal with this difficulty. The first type of methods can be viewed as special cases of MM algorithm [14] or of multi-stage convex relaxation [15], such as local quadratic approximation (LQA) of the penalty [12] and local linear approximation (LLA) of the the penalty [16]. Such algorithms generate a solution sequence $\{\beta^k\}_k$ that can guarantee the convergence of the objective functions, but the convergence property of $\{\beta^k\}_k$ is generally unknown. Moreover, the cost per iteration of this type of algorithms is the cost of a LASSO solver. The second type of method includes coordinate descent (CD) type algorithms [17], [18]. The best convergence result for CD algorithms for minimizing (5) is that any cluster point of $\{\beta^k\}_k$ must be a stationary point of (6) and (7) [17], [18]. As shown in [17], [18], CD-type algorithms are faster than the first type of algorithms mentioned above, because the cost per iteration of CD algorithms is only $O(np)$. However, when high accuracy is pursued CD-type algorithms may need lots of iterations, since its convergence speed is sub-linear numerically or linearly locally [19].

In this paper we develop a local but superlinearly convergent algorithm for minimizing (5) with the SCAD and the MCP. To this end, we first establish that the global minimizers of (5) with the SCAD penalty (6) and MCP (7) are roots of the nonsmooth KKT equations. Conversely we show that any root of the KKT equations is at least a global coordinate-wise minimizer and stationary point of (5). Then we adopt Semi-smooth Newton (SSN) algorithm [20], [21], [22] to solve the nonsmooth KKT equations. We establish the locally superlinear convergence property of SSN. Furthermore, computational complexity analysis shows that the cost of each iteration in SSN is at most $O(np)$, which is the same as coordinate descent. Hence, for a given λ, γ , the overall cost of using SSN to find a (local) minimizer of (5) is still $O(np)$, since SSN always converges after only a few iterations if it is warm-started. Thus SSN is possibly one of the fastest and most accurate algorithms for computing the whole solution path of (5) by running SSN repeatedly at some given $\lambda_k, k = 1, 2, \dots, M$ with warm start.

Numerical simulation results comparing with CD algorithms also verify this.

The remainder of this paper is organized as follows. In Section 2 we describe the Semi-smooth Newton (SSN) algorithm. In Section 3 we establish the superlinear convergence property and analyze its computational complexity. Implementation detail and numerical comparison with coordinate descent (CD) algorithm on simulated and real data examples are given in Section 4. We conclude in Section 5 with comments and future work.

II. SEMI-SMOOTH NEWTON ALGORITHM FOR PENALIZED REGRESSION

A. Notation and Background on Newton Derivative

We first introduce the notation used throughout this paper and describe the concept and properties of Newton's derivative [20], [21], [23], [22].

For a column vector $\beta = (\beta_1, \beta_2, \dots, \beta_p)^T \in \mathbb{R}^p$, denote its q -norm by $\|\beta\|_q = (\sum_{i=1}^p |\beta_i|^q)^{\frac{1}{q}}$, $q \in [1, \infty)$, and denote its ℓ_0 - and ℓ_∞ - norm by $\|\beta\|_0 = |\{i : \beta_i \neq 0, 1 \leq i \leq p\}|$ and $\|\beta\|_\infty = \max_{1 \leq i \leq p} |\beta_i|$, respectively. X^T is the transpose of the feature matrix $X \in \mathbb{R}^{n \times p}$, and $\|X\|$ denotes the operator norm of X induced by the vector 2-norm. The matrix X is assumed to be columnwise normalized, i.e., $\|X_i\|_2 = 1$ for $i = 1, 2, \dots, p$. $\mathbf{1}$ or $\mathbf{0}$ denote a column vector or a matrix with elements all 1 or 0. Define $S = \{1, 2, \dots, p\}$. For any $A \subseteq S$ with cardinality $|A|$, denote $\beta_A \in \mathbb{R}^{|A|}$ (or $X_A \in \mathbb{R}^{|A| \times p}$) as the subvector (or submatrix) whose entries (or columns) are listed in A . And X_{AB} denotes submatrix of X whose rows and columns are listed in A and B respectively. $\text{supp}(\beta)$ denotes the support of β , and $\text{sign}(z)$ denotes the entry-wise sign of a given vector z .

Let $F : \mathbb{R}^m \rightarrow \mathbb{R}^l$ be a nonlinear map. [20], [21], [23], [22] generalized the classical Newton-Raphson algorithm to find a root of $F(z) = \mathbf{0}$, when F is not Fréchet differentiable but only Newton differentiable in the following sense.

Definition 1: $F : \mathbb{R}^m \rightarrow \mathbb{R}^l$ is called Newton differentiable at $x \in \mathbb{R}^m$ if there exists an open neighborhood $N(x)$ and a family of mappings $D : N(x) \rightarrow \mathbb{R}^{l \times m}$ such that

$$\|F(x+h) - F(x) - D(x+h)h\|_2 = o(\|h\|_2) \quad \text{for } \|h\|_2 \rightarrow 0.$$

The set of mappings $\{D(z) : z \in N(x)\}$ denoted by $\nabla_N F(x)$ is called Newton derivative of F at x .

It can be easily seen that $\nabla_N F(x)$ coincides with the Fréchet derivative at x if F is continuously Fréchet differentiable. Let $F_i : \mathbb{R}^m \rightarrow \mathbb{R}^1$ be Newton differentiable at x with Newton derivative $\nabla_N F_i(x)$, $i = 1, 2, \dots, l$, then $F = (F_1, F_2, \dots, F_l)^T$ is also Newton differentiable at x with Newton derivative

$$\nabla_N F(x) = (\nabla_N F_1(x), \nabla_N F_2(x), \dots, \nabla_N F_l(x))^T. \quad (9)$$

Furthermore, if both F and H are Newton differentiable at x then any linear combination of them is also Newton differentiable at x , i.e., for any $\theta, \mu \in \mathbb{R}^1$

$$\nabla_N(\theta F + \mu G)(x) = \theta \nabla_N F(x) + \mu \nabla_N G(x) \quad (10)$$

Let $H : \mathbb{R}^s \rightarrow \mathbb{R}^l$ be Newton differentiable with Newton derivative $\nabla_N H$. Let $L \in \mathbb{R}^{s \times m}$ and define $F(x) = H(Lx + z)$ for any given $z \in \mathbb{R}^s$. Then it is easy to check by definition that the chain rule holds, i.e., $F(x)$ is Newton differentiable at x with Newton derivative

$$\nabla_N F(x) = \nabla_N H(Lx + z)L. \quad (11)$$

In Lemma 2 we will give two important thresholding functions which are Newton differentiable but not Fréchet differentiable.

B. Optimality Conditions and Semi-smooth Newton Algorithm

In this subsection, we give a necessary condition for the global minimizers of (5) with the SCAD penalty (6) or the MCP (7). Specifically, we show that the global minimizers satisfy a set of KKT equations, which are nonsmooth but are Newton differentiable equations. Then we use Semi-smooth Newton algorithm to solve it.

Now we derive the optimality conditions of the minimizers of (5) with $p(z; \lambda, \gamma)$ to be $p_{\text{scad}}(z; \lambda, \gamma)$ or $p_{\text{mcp}}(z; \lambda, \gamma)$. This notation will be used in the rest of the paper for simplicity.

For a given $t \in \mathbb{R}^1$, let

$$T(t; \lambda, \gamma) = \arg \min_{z \in \mathbb{R}^1} \frac{1}{2}(z - t)^2 + p(z; \lambda, \gamma). \quad (12)$$

be the thresholding functions corresponding to penalty $p(z; \lambda, \gamma)$, which have a closed form for both SCAD and MCP penalties [17], [18].

Lemma 1: Let $T(t; \lambda, \gamma)$ be defined in (12). Then for $p = p_{\text{mcp}}$,

$$T_{\text{mcp}}(t; \lambda, \gamma) = \begin{cases} \frac{S(t; \lambda)}{1 - 1/\gamma}, & \text{if } |t| \leq \gamma\lambda, \\ t, & \text{if } |t| > \gamma\lambda. \end{cases} \quad (13)$$

and for $p = p_{\text{scad}}$,

$$T_{\text{scad}}(t; \lambda, \gamma) = \begin{cases} S(t; \lambda), & \text{if } |t| \leq 2\lambda, \\ \frac{S(t; \lambda\gamma/(\gamma - 1))}{1 - 1/(\gamma - 1)}, & \text{if } 2\lambda < |t| \leq \gamma\lambda, \\ t, & \text{if } |t| > \gamma\lambda. \end{cases} \quad (14)$$

respectively, where the scalar function $S(t; \lambda) = \max\{|t| - \lambda, 0\}\text{sign}(t)$ is the soft-thresholding function [24].

Proof: See Appendix A. \blacksquare

The following KKT condition shows that the global minimizers of (5) satisfy a nonsmooth equation which is the basis of our Semi-smooth Newton algorithm.

Theorem 1: Let $\hat{\beta}$ be a global minimizer of (5). Then there exists $\hat{d} \in \mathbb{R}^p$ such that the following optimality conditions hold,

$$\hat{d} = \tilde{y} - G\hat{\beta}, \quad (15)$$

$$\hat{\beta} = \mathbb{T}(\hat{\beta} + \hat{d}; \lambda, \gamma). \quad (16)$$

where $G = X^T X$, $\tilde{y} = X^T y$, for a given vector $z \in \mathbb{R}^p$, $\mathbb{T}(z; \lambda, \gamma)$ is the thresholding operator operates on z component-wise by (12).

Conversely, if there exists $(\hat{\beta}, \hat{d})$ satisfying (15) - (16), then $\hat{\beta}$ is a stationary point of (5).

Proof: See Appendix B. \blacksquare

Let

$$F(\beta; d) = \begin{bmatrix} F_1(\beta; d) \\ F_2(\beta; d) \end{bmatrix} : \mathbb{R}^p \times \mathbb{R}^p \rightarrow \mathbb{R}^{2p}, \quad (17)$$

where $F_1(\beta; d) := \beta - \mathbb{T}(\hat{\beta} + \hat{d}; \lambda, \gamma)$, and $F_2(\beta; d) := G\beta + d - \tilde{y}$. For simplicity, we refer to F as a KKT function. By Theorem 1, the global minimizers of (5) are roots of $F(\beta; d)$. And the roots of $F(\beta; d)$ are stationary points of (5). The difficulty is that the thresholding operators corresponding concave penalties including the SCAD and the MCP are not differentiable which in turn results in the non-differentiability of F . So we resort to the semi-smooth Newton method (SSN) [20], [21], [23], [22].

Let $z = (\beta; d)$. At the k th iteration, the semi-smooth Newton method for finding the root of $F(z) = 0$ consists of two steps.

- (1) Solve $H^k \delta^k = -F(z^k)$ for δ^k , where H^k is an element of $\nabla_N F(z^k)$.
- (2) Update $z^{k+1} = z^k + \delta^k$, set $k \leftarrow k + 1$ and go to step (1).

This has the same form as the classical Newton method, except that here we use an element of $\nabla_N F(z^k)$ in step (1). Indeed, the key to the success of this method is to find a suitable and invertible H^k . We state this method in Algorithm 1.

Algorithm 1 Semi-smooth Newton algorithm for finding a root z^* of $F(z)$

- 1: Input: initial guess z^0 . Set $k = 0$.
- 2: **for** $k = 0, 1, 2, 3, \dots$ **do**
- 3: Choose $H^k \in \nabla_N F(z^k)$.
- 4: Get the Semi-smooth Newton direction δ^k by solving

$$H^k \delta^k = -F(z^k). \quad (18)$$

- 5: Update $z^{k+1} = z^k + \delta^k$.
- 6: Stop or $k := k + 1$.
- 7: **end for**
- 8: Output: \hat{z} as an estimation of z^* .

C. The Newton Derivatives of the KKT Functions

Denote the KKT functions as defined in (17) by F_{scad} and F_{mcp} for the SCAD and the MCP, respectively. To compute the roots of F_{mcp} and F_{scad} based on the SSN, we need to calculate their Newton derivatives.

Lemma 2: $T_{\text{mcp}}(t; \lambda, \gamma)$ and $T_{\text{scad}}(t; \lambda, \gamma)$ are Newton differentiable with respect to t with Newton derivatives

$$\nabla_N T_{\text{mcp}}(t) = \begin{cases} 0, & |t| < \lambda, \\ r \in \mathbb{R}^1, & |t| = \lambda, \\ 1/(1-1/\gamma), & \lambda < |t| < \gamma\lambda, \\ r \in \mathbb{R}^1, & |t| = \gamma\lambda, \\ 1, & \gamma\lambda < |t|, \end{cases} \quad (19)$$

and

$$\nabla_N T_{\text{scad}}(t) = \begin{cases} 0, & |t| < \lambda, \\ r \in \mathbb{R}^1, & |t| = \lambda, \\ 1, & \lambda < |t| < 2\lambda, \\ r \in \mathbb{R}^1, & |t| = 2\lambda, \\ 1/(1-1/(\gamma-1)), & 2\lambda < |t| < \gamma\lambda, \\ r \in \mathbb{R}^1, & |t| = \gamma\lambda, \\ 1, & \gamma\lambda < |t|, \end{cases} \quad (20)$$

respectively.

Proof: See Appendix C. \blacksquare

1) *The Newton derivative of F_{mcp} :* Consider the KKT function F_{mcp} . For any given point $z^k = (\beta^k; d^k) \in \mathbb{R}^{2p}$, define

$$A_k^1 = \{i \in S : \lambda < |\beta_i^k + d_i^k| < \lambda\gamma\}, \quad (21)$$

$$A_k^2 = \{i \in S : |\beta_i^k + d_i^k| \geq \lambda\gamma\}, \quad (22)$$

$$A_k = A_k^1 \cup A_k^2, \quad (23)$$

$$B_k = \{i \in S : |\beta_i^k + d_i^k| \leq \lambda\}. \quad (24)$$

We rearrange the order of the entries of z^k as follows:

$$z_{\text{mcp}}^k = (\beta_{A_k^1}^k; d_{A_k^1}^k; \beta_{B_k}^k; d_{A_k^2}^k; \beta_{A_k^2}^k; d_{B_k}^k).$$

Denote the Newton derivative of F_{mcp} at z_{mcp}^k as $\nabla_N F_{\text{mcp}}(z_{\text{mcp}}^k)$. In Theorem 2, we will show that $H_{\text{mcp}}^k \in \nabla_N F_{\text{mcp}}(z_{\text{mcp}}^k)$, where, $H_{\text{mcp}}^k \in \mathbb{R}^{p \times p}$ is given by

$$H_{\text{mcp}}^k = \begin{bmatrix} H_{11}^k & H_{12}^k \\ H_{21}^k & H_{22}^k \end{bmatrix} \quad (25)$$

with

$$H_{11}^k = \begin{bmatrix} -\frac{1}{\gamma-1} I_{A_k^1 A_k^1} & \mathbf{0} & \mathbf{0} \\ \mathbf{0} & -I_{A_k^2 A_k^2} & \mathbf{0} \\ \mathbf{0} & \mathbf{0} & I_{B_k B_k} \end{bmatrix},$$

$$H_{12}^k = \begin{bmatrix} -\frac{\gamma}{\gamma-1} I_{A_k^1 A_k^1} & \mathbf{0} & \mathbf{0} \\ \mathbf{0} & \mathbf{0} & \mathbf{0} \\ \mathbf{0} & \mathbf{0} & \mathbf{0} \end{bmatrix},$$

$$H_{21}^k = \begin{bmatrix} G_{A_k^1 A_k^1} & \mathbf{0} & G_{A_k^1 B_k} \\ G_{A_k^2 A_k^1} & I_{A_k^2 A_k^2} & G_{A_k^2 B_k} \\ G_{B_k A_k^1} & \mathbf{0} & G_{B_k B_k} \end{bmatrix},$$

$$H_{22}^k = \begin{bmatrix} I_{A_k^1 A_k^1} & G_{A_k^1 A_k^2} & \mathbf{0} \\ \mathbf{0} & G_{A_k^2 A_k^2} & \mathbf{0} \\ \mathbf{0} & G_{B_k A_k^2} & I_{B_k B_k} \end{bmatrix}.$$

2) *The Newton derivative of F_{scad} :* Now consider the KKT function F_{scad} . For any given point $z^k = (\beta^k; d^k) \in \mathbb{R}^{2p}$, define

$$A_k^1 = \{i \in S : \lambda < |\beta_i^k + d_i^k| < 2\lambda\}, \quad (26)$$

$$A_k^2 = \{i \in S : 2\lambda \leq |\beta_i^k + d_i^k| < \lambda\gamma\}, \quad (27)$$

$$A_k^3 = \{i \in S : |\beta_i^k + d_i^k| \geq \lambda\gamma\}, \quad (28)$$

$$A_k = A_k^1 \cup A_k^2 \cup A_k^3, \quad (29)$$

$$B_k = \{i \in S : |\beta_i^k + d_i^k| \leq \lambda\}. \quad (30)$$

We rearrange the entries of z_{scad} as follows:

$$z_{\text{scad}}^k := (\beta_{B_k}^k; d_{A_k^1}^k; \beta_{A_k^2}^k; d_{A_k^3}^k; d_{B_k}^k; \beta_{A_k^1}^k; d_{A_k^2}^k; \beta_{A_k^3}^k).$$

Denote the Newton derivative of F_{scad} at z_{scad}^k as $\nabla_N F_{\text{scad}}(z_{\text{scad}}^k)$. In Theorem 2, we will show that $H_{\text{scad}}^k \in \nabla_N F_{\text{scad}}(z_{\text{scad}}^k)$, where, $H_{\text{scad}}^k \in \mathbb{R}^{p \times p}$ is given by

$$H_{\text{scad}}^k := \begin{bmatrix} H_{11}^k & H_{12}^k \\ H_{21}^k & H_{22}^k \end{bmatrix} \quad (31)$$

with

$$H_{11}^k = \begin{bmatrix} I_{B_k B_k} & \mathbf{0} & \mathbf{0} & \mathbf{0} \\ \mathbf{0} & -I_{A_k^1 A_k^1} & \mathbf{0} & \mathbf{0} \\ \mathbf{0} & \mathbf{0} & -\frac{1}{\gamma-2} I_{A_k^2 A_k^2} & \mathbf{0} \\ \mathbf{0} & \mathbf{0} & \mathbf{0} & -I_{A_k^3 A_k^3} \end{bmatrix},$$

$$H_{12}^k = \begin{bmatrix} \mathbf{0} & \mathbf{0} & \mathbf{0} & \mathbf{0} \\ \mathbf{0} & \mathbf{0} & \mathbf{0} & \mathbf{0} \\ \mathbf{0} & \mathbf{0} & -\frac{\gamma-1}{\gamma-2} I_{A_k^2 A_k^2} & \mathbf{0} \\ \mathbf{0} & \mathbf{0} & \mathbf{0} & \mathbf{0} \end{bmatrix},$$

$$H_{21}^k = \begin{bmatrix} G_{B_k B_k} & \mathbf{0} & G_{B_k A_k^2} & \mathbf{0} \\ G_{A_k^1 B_k} & I_{A_k^1 A_k^1} & G_{A_k^1 A_k^1} & \mathbf{0} \\ G_{A_k^2 B_k} & \mathbf{0} & G_{A_k^2 A_k^2} & \mathbf{0} \\ G_{A_k^3 B_k} & \mathbf{0} & G_{A_k^3 A_k^2} & I_{A_k^3 A_k^3} \end{bmatrix},$$

$$H_{22}^k = \begin{bmatrix} I_{B_k B_k} & G_{B_k A_k^1} & \mathbf{0} & G_{B_k A_k^3} \\ \mathbf{0} & G_{A_k^1 A_k^1} & \mathbf{0} & G_{A_k^1 A_k^3} \\ \mathbf{0} & G_{A_k^2 A_k^1} & I_{A_k^2 A_k^2} & G_{A_k^2 A_k^3} \\ \mathbf{0} & G_{A_k^3 A_k^1} & \mathbf{0} & G_{A_k^3 A_k^3} \end{bmatrix}.$$

Theorem 2: Both F_{mcp} and F_{scad} are Newton differentiable at z_{mcp}^k and z_{scad}^k with

$$H_{\text{mcp}}^k \in \nabla_N F_{\text{mcp}}(z_{\text{mcp}}^k),$$

and

$$H_{\text{scad}}^k \in \nabla_N F_{\text{scad}}(z_{\text{scad}}^k).$$

Furthermore, the inverse of H_{mcp}^k and H_{scad}^k are uniformly bounded with

$$\|(H_{\text{mcp}}^k)^{-1}\| \leq M_\gamma,$$

and

$$\|(H_{\text{scad}}^k)^{-1}\| \leq M_\gamma,$$

where, $M_\gamma = (3\gamma + 2) + (\gamma + 1)(2\gamma + 5)$.

Proof: See Appendix D. \blacksquare

With the Newton derivative at hand we can apply SSN to compute the roots of F_{mcp} and F_{scad} . Here we give the details for F_{mcp} . By the definitions of A_k^1, A_k^2, I_k and T_{mcp} , we get

$$F_{\text{mcp}}(z_{\text{mcp}}^k) = \begin{bmatrix} \beta_{A_k^1}^k - \frac{\gamma}{\gamma-1}(\beta_{A_k^1}^k + d_{A_k^1}^k - \lambda \text{sign}(\beta_{A_k^1}^k + d_{A_k^1}^k)) \\ \beta_{A_k^2}^k - (\beta_{A_k^2}^k + d_{A_k^2}^k) \\ \beta_{B_k}^k \\ G_{A_k^1 A_k^1} \beta_{A_k^1}^k + G_{A_k^1 A_k^2} \beta_{A_k^2}^k + G_{A_k^1 B_k} \beta_{B_k}^k + d_{A_k^1}^k - \tilde{y}_{A_k^1} \\ G_{A_k^2 A_k^1} \beta_{A_k^1}^k + G_{A_k^2 A_k^2} \beta_{A_k^2}^k + G_{A_k^2 B_k} \beta_{B_k}^k + d_{A_k^2}^k - \tilde{y}_{A_k^2} \\ G_{B_k A_k^1} \beta_{A_k^1}^k + G_{B_k A_k^2} \beta_{A_k^2}^k + G_{B_k B_k} \beta_{B_k}^k + d_{B_k}^k - \tilde{y}_{B_k} \end{bmatrix}. \quad (32)$$

Substituting (32) and (25) into the Semi-smooth Newton direction equation

$$H_{\text{mcp}}^k \delta_{\text{mcp}}^k = -F_{\text{mcp}}(z_{\text{mcp}}^k)$$

and observing the update relation

$$z_{\text{mcp}}^{k+1} = z_{\text{mcp}}^k + \delta_{\text{mcp}}^k,$$

we get (after some tedious algebraic simplifications)

$$d_{A_k^2}^{k+1} = \mathbf{0}, \quad (33)$$

$$\beta_{B_k}^{k+1} = \mathbf{0}, \quad (34)$$

$$\tilde{G}_{A_k A_k} \beta_{A_k}^{k+1} = s_{A_k}, \quad (35)$$

$$d_{A_k^1}^{k+1} = -\beta_{A_k}^{k+1}/\gamma + s_{A_k^1}, \quad (36)$$

$$d_{B_k}^{k+1} = \tilde{y}_{B_k} - G_{B_k A_k} \beta_{A_k}^{k+1}, \quad (37)$$

where,

$$\tilde{G}_{A_k A_k} = G_{A_k A_k} - \begin{bmatrix} I_{A_k^1 A_k^1}/\gamma & \mathbf{0} \\ \mathbf{0} & \mathbf{0} \end{bmatrix}, \quad (38)$$

$$s_{A_k^1} = \lambda \text{sign}(\beta_{A_k^1}^k + d_{A_k^1}^k), \quad (39)$$

$$s_{A_k} = \tilde{y}_{A_k} - \begin{bmatrix} s_{A_k^1} \\ \mathbf{0} \end{bmatrix}. \quad (40)$$

We summarize the above in the following algorithm.

Algorithm 2 Semi-Smooth Newton algorithm for finding a root of F_{mcp}

- 1: Input: X, y, λ, γ , initial guess $(\beta^0; d^0)$. Set $k = 0$.
- 2: Pre-compute $\tilde{y} = X^T y$ and store it.
- 3: **for** $k = 0, 1, 2, 3, \dots$ **do**
- 4: Compute A_k^1, A_k^2, A_k, B_k by (21) - (24).
- 5: $\beta_{B_k}^{k+1} = \mathbf{0}$.
- 6: $d_{A_k^2}^{k+1} = \mathbf{0}$.
- 7: Compute $\tilde{G}_{A_k A_k}, s_{A_k^1}, s_{A_k}$ by (38)-(40).
- 8: $\beta_{A_k}^{k+1} = \tilde{G}_{A_k A_k}^{-1} s_{A_k}$.
- 9: $d_{A_k^1}^{k+1} = -\beta_{A_k}^{k+1}/\gamma + s_{A_k^1}$,
- 10: $d_{B_k}^{k+1} = \tilde{y}_{B_k} - G_{B_k A_k} \beta_{A_k}^{k+1}$.
- 11: Check Stop condition
- If stop
- Denote the last iteration by $\beta_{\hat{A}}, \beta_{\hat{B}}, d_{\hat{A}}, d_{\hat{B}}$.
- Else
- $k := k + 1$.
- 12: **end for**
- 13: Output: $\hat{\beta} = (\beta_{\hat{A}}; \beta_{\hat{B}})$, $\hat{d} = (d_{\hat{A}}; d_{\hat{B}})$.

The Semi-smooth Newton algorithm for F_{scad} can be constructed in a similar fashion. Let

$$\tilde{G}_{A_k A_k} := G_{A_k A_k} - \begin{bmatrix} \mathbf{0} & \mathbf{0} & \mathbf{0} \\ \mathbf{0} & I_{A_k^2 A_k^2}/(\gamma - 1) & \mathbf{0} \\ \mathbf{0} & \mathbf{0} & \mathbf{0} \end{bmatrix}, \quad (41)$$

$$s_{A_k^2} := \frac{\gamma \lambda}{\gamma - 1} \text{sign}(\beta_{A_k^2}^k + d_{A_k^2}^k), \quad (42)$$

$$s_{A_k} := \tilde{y}_{A_k} - \begin{bmatrix} d_{A_k^1}^{k+1} \\ s_{A_k^2} \\ \mathbf{0} \end{bmatrix}. \quad (43)$$

Then the algorithm for solving $F_{scad}(z) = 0$ is as follows.

Algorithm 3 Semi-Smooth Newton algorithm for finding a root of F_{scad}

- 1: Input: X, y, λ, γ , initial guess $(\beta^0; d^0)$. Set $k = 0$.
- 2: Pre-compute $\tilde{y} = X^T y$ and store it.
- 3: **for** $k = 0, 1, 2, 3, \dots$ **do**
- 4: Compute $A_k^1, A_k^2, A_k^3, A_k, B_k$ by (26) - (30).
- 5: $\beta_{B_k}^{k+1} = \mathbf{0}$.
- 6: $d_{A_k^1}^{k+1} = \lambda \text{sign}(\beta_{A_k^1}^k + d_{A_k^1}^k)$.
- 7: $d_{A_k^3}^{k+1} = \mathbf{0}$.
- 8: Compute $\tilde{G}_{A_k A_k}, s_{A_k^2}, s_{A_k}$ by (41)-(43).
- 9: $\beta_{A_k}^{k+1} = \tilde{G}_{A_k A_k}^{-1} s_{A_k}$.
- 10: $d_{A_k^2}^{k+1} = -\beta_{A_k}^{k+1}/(\gamma - 1) + s_{A_k^2}$,
- 11: $d_{B_k}^{k+1} = \tilde{y}_{B_k} - G_{B_k A_k} \beta_{A_k}^{k+1}$.
- 12: Check Stop condition
- If stop
- Denote the last iteration by $\beta_{\hat{A}}, \beta_{\hat{B}}, d_{\hat{A}}, d_{\hat{B}}$.
- Else
- $k := k + 1$.
- 13: **end for**
- 14: Output: $\hat{\beta} = (\beta_{\hat{A}}; \beta_{\hat{B}})$, $\hat{d} = (d_{\hat{A}}; d_{\hat{B}})$.

A natural stopping criterion for both algorithms is when $A_k = A_{k+1}$ holds for some k , which can be checked inexpensively. We also stop them when the iteration k exceeds some given positive integer J as a safeguard.

Remark 1: Here we give some discussions on the requirement for the design matrix X and the sparsity level of β^\dagger . It is obvious that Algorithm 2 and Algorithm 3 are well-defined if $\tilde{G}_{A_k A_k}$ in (38) and (41) are invertible respectively. Sufficient conditions to guarantee these are

$$\kappa_-(|A_k|) > 1/\gamma \quad (44)$$

and

$$\kappa_-(|A_k|) > 1/(\gamma - 1), \quad (45)$$

respectively, where

$$\kappa_-(|A_k|) = \min_{\|z\|=1, \|z\|_0 \leq |A_k|} \|Xz\|^2$$

denotes the smallest sparse eigenvalues of X with order $|A_k|$ [25]. Therefor, we need the assumption that the smallest singular value of the submatrixes of X_{A_k} bound away from $1/\gamma$ ($1/(\gamma - 1)$) to guarantee the well-posedness of the proposed algorithms. This assumption is reasonable since the size of the active set A_k is small, which is thanks to the underlying sparsity level $\|\beta^\dagger\|_0$ is much smaller than the number of samples n .

III. CONVERGENCE, COMPLEXITY ANALYSIS AND SOLUTION PATH

In this subsection, following [20], [21], [23], [22], we will establish the local superlinear convergence result of Algorithms 2 and 3, which are similar to the classical Newton algorithm, and analyze their computational complexity, and make discussion and comparison with existing related works.

A. Convergence Analysis

Theorem 3: Let β_{mcp}^k and β_{scad}^k be generated by Algorithms 2 and 3, respectively. Then, β_{mcp}^k and β_{scad}^k converge locally and superlinearly to point satisfying equation (15) - (16).

Proof: See Appendix E. \blacksquare

Remark 2: By Theorem 1 we can see Algorithms 2 and 3 also converge locally and superlinearly to a stationary points of (5) with the MCP (7) and SCAD penalty (6), respectively.

B. Computational Complexity

We now consider the number of floating point operations per iteration. It takes $O(p)$ flops to finish step 4-7 (step 4-8) in Algorithm 2 (Algorithm 3). For step 8 (step 9) in Algorithm 2 (Algorithm 3), inverting the positive definite matrix $\tilde{G}_{A_k A_k}$ by Cholesky factorization takes $O(|A_k|^3)$ flops. As for step 9-10 (10-11) in Algorithm 2 (Algorithm 3), $O(np)$ flops are enough to finish the matrix-vector product. So the the overall cost per iteration for Algorithms 2 and Algorithm 3 is $O(\max(|A_k|^3, np))$. Numerically $|A_k|$ usually increases and converges to $O(\|\beta^\dagger\|_0)$ if the algorithm is warm started. Therefore, if the underling solution is sufficiently sparse such that $\|\beta^\dagger\|_0^3 \leq O(np)$ then it takes $O(np)$ flops per iteration for both algorithms. Hence the overall cost of Algorithms 2 and 3 are still $O(np)$ due to their superlinear convergence. The computational complexity analysis shows that it is very fast to use Algorithm 2 and 3 to compute the solution paths with warm starts. This is supported by the numerical results presented in Section 4.

The computational cost of coordinate descent algorithm [17], [18] and iterative thresholding algorithm [26] for (6) and (7) is also $O(np)$ per iteration. The cluster points of sequences generated by CD and iterative thresholding also satisfy (15)-(16). But the convergence rate of these two type of algorithms is at best sub-linear even in the case of LASSO penalized problem where the object function is convex [27]. Hence it is not surprising that Algorithms 2 and 3 outperform CD-type algorithms in accuracy and efficiency, see, numerical results in Section 4.

C. Solution Path

An important issue in implementing a Newton-type algorithm is how to choose an initial value. We use warm start to determine the initial value. This strategy has been successfully used for computing the LASSO and the Enet paths [7]. It is also a simple but powerful tool to handle the local convergence of concavely penalized regression problems [17], [18], [28]. Hence we use warm start to generate the solution path on an interval of the penalty parameter λ . The locally superlinear convergence results in Theorem 3 guarantee that after a small number of iterations we will get an approximate solution with high accuracy if the algorithms are warm started.

We are also often interested in the whole solution path $\hat{\beta}(\lambda)$ for $\lambda \in [\lambda_{\min}, \lambda_{\max}]$, where $0 < \lambda_{\min} < \lambda_{\max}$ are two prespecified numbers. This will be needed for selecting the λ value based on a data driven procedure such as

cross validation or bayesian information criterion. Here we approximate the solution path by computing $\hat{\beta}(\lambda)$ on a given finite set $\Lambda = \{\lambda_0, \lambda_1, \dots, \lambda_M\}$ for some integer M , where $\lambda_0 > \lambda_1 > \dots > \lambda_M > 0$. Obviously, $\hat{\beta}(\lambda) = \mathbf{0}$ satisfies (15) and (16) if $\lambda \geq \|X^T y\|_\infty$. Hence we set $\lambda_{\max} = \lambda_0 = \|X^T y\|_\infty$, $\lambda_t = \lambda_0 \rho^t$, $t = 0, 1, \dots, M$, and $\lambda_{\min} = \lambda_0 \rho^M$, where $\rho \in (0, 1)$. On the decreasing sequence $\{\lambda_t\}_t$, we use the solution at λ_t as the initial value for computing the solution at λ_{t+1} , which is referred as the warmstarting (or continuation) technique. See [29], [28], [30], [31], [32] and references therein for more details.

Remark 3: In practice, we let $\lambda_{\min} = \alpha \lambda_{\max}$ for a small α , and then divide the interval $[\lambda_{\min}, \lambda_{\max}]$ into M equally distributed subintervals in the logarithmic scale. For a given α , ρ is determined by M and a large M implies a large ρ . Unless otherwise specified, we set $\alpha = 1e-5$ and $M = 100$. Equivalently, $\rho = \exp\{-[\log(1) - \log(\alpha)]/M\} \approx 0.9$. Due to the locally superlinear convergence property of SSN and the warmstarting technique on the solution path, the maximal iteration number J could be a small positive integer. We recommend $J \leq 5$ and the choice $J = 1$ generally works well in practice.

To decide the “optimal” choice of λ , a high-dimensional Bayesian information criterion (HBIC) [33], [34] can be utilized. In this paper, we also propose to use a novel voting selection criterion (VSC) [32], [35] for choosing the optimal value of tuning parameter. Assume we run the SSN Algorithm to yield a solution path until, for example, $\|\hat{\beta}(\lambda_t)\|_0 > \lfloor n/\log(p) \rfloor$ for some t , say $t = W$ ($W \leq M$). Let

$$\Lambda_\ell = \{\lambda_t : \|\hat{\beta}(\lambda_t)\|_0 = \ell, t = 1, \dots, W\},$$

where $\ell = 1, \dots, \lfloor n/\log(p) \rfloor$ is the set of tuning parameter at which the output of SSN has ℓ nonzero elements. Then we determine λ by VSC as

$$\bar{\ell} = \arg \max_{\ell} \{|\Lambda_\ell|\} \quad \text{and} \quad \hat{\lambda} = \min\{\Lambda_{\bar{\ell}}\}. \quad (46)$$

It is noteworthy that the VSC (or HBIC) selector is seamlessly integrated with the warmstarting technique without any extra computational overhead, since the sequence $\{\hat{\beta}(\lambda_t)\}$ is already generated along the warmstarting solution path.

Remark 4: Both the HBIC and the VSC selectors work well in our numerical examples. When the assumption of linear model is satisfied, numerical results show that VSC is slightly more accurate than HBIC. Thus one can use either HBIC or VSC to find a solution for simulated data, while it is suggested to use the HBIC for real-world data.

D. Discussion with DC Newton-type Algorithm

In [36], the authors propose a DC proximal Newton (DCPN) method to solve nonconvex sparse learning problems with general nonlinear loss functions. They rewrite the nonconvex penalties into difference of two convex functions and use multistage convex relaxation to transform the original optimization into sequences of LASSO regularized nonlinear regressions. At each stage, they propose to use the second order Taylor expansion to approximate the nonlinear loss functions, and then use the coordinate descent with active set strategy [37]

to solve the deduced LASSO regularized linear regressions, which is called proximal Newton step by the authors. Inspired by the previous work on using nonsmooth Newton methods to find roots of nonsmooth equations [20], [21], [22], [38], we first derive the nonsmooth KKT equations of the optimal solution of the target nonconvex optimization problems, and then propose to use the Semi-smooth Newton (SSN) method to solve the KKT equations directly. The proximal Newton method serves as an inner solver in [36], while the SSN method solves the nonconvex optimization directly via finding roots of the KKT equations. Hence, it is no surprise that the SSN algorithm is generally faster than the DCPN algorithm with approximately the same estimation error. See Section IV-D for the numerical comparison.

In [36], the authors prove an elegant non-asymptotic statistical estimator error on the solution path (the error between the output of their algorithms at each tuning parameter and the underlying true regression coefficient) via restricted strong convexity assumptions. We prove the local superlinear convergence of SSN (the output of SSN converges locally and superlinearly to the KKT points). Therefore, the work of [36] mainly focuses on the statistical estimation error while we care more about the convergence rate from the optimization perspective.

IV. NUMERICAL EXAMPLES

In this section we present numerical examples to illustrate the performance of the proposed SSN algorithm. All the experiments are performed in MATLAB R2010b and R version 3.3.2 on a quad-core laptop with an Intel Core i5 CPU (2.60 GHz) and 8 GB RAM running Windows 8.1 (64 bit).

A. Implementation Setting

We generate synthetic data from (1). The rows of the $n \times p$ matrix X are sampled as i.i.d. copies from $N(\mathbf{0}, \Sigma)$ with $\Sigma = (r^{|j-k|})$, $1 \leq j, k \leq p$, where r is the correlation coefficient of X . The noise vector ε is generated independently from $N(\mathbf{0}, \sigma^2 I_n)$, where σ is the noise level. The underlying regression coefficient vector β^\dagger is a random sparse vector chosen as T -sparse (i.e., $T = \|\beta^\dagger\|_0$) with a dynamic range (DR) given by

$$\text{DR} := \frac{\max\{|\beta_i^\dagger| : \beta_i^\dagger \neq 0\}}{\min\{|\beta_i^\dagger| : \beta_i^\dagger \neq 0\}} = 10. \quad (47)$$

Let $\mathcal{A} = \{i : \beta_i^\dagger \neq 0\}$ be the true model and $\widehat{\mathcal{A}} = \{i : \widehat{\beta}_i \neq 0\}$ be the estimated model. Following [39], each nonzero entry of β^\dagger is generated as follows:

$$\beta_i^\dagger = \eta_{1i} 10^{\eta_{2i}}, \quad (48)$$

where $i \in \mathcal{A}$, $\eta_{1i} = \pm 1$ with probability $\frac{1}{2}$ and η_{2i} is uniformly distributed in $[0, 1]$. Then the outcome vector y is generated via $y = X\beta^\dagger + \varepsilon$. For convenience, we use (n, p, r, σ, T) to denote the data generated as above.

Unless otherwise stated, we set $\gamma = 3.7$ and $\gamma = 2.7$ for SCAD and MCP respectively, as suggested by [12] and [13].

B. The Convergence Behavior of the SSN Algorithm

We give an example to illustrate the warmstarting technique and local superlinear convergence of the SSN algorithm. To this end, we generate a simulated dataset ($n = 200, p = 1000, r = 0.1, \sigma = 0.01, T = 20$). To save space, we only consider the SCAD penalty since similar phenomenon happens for the MCP penalty. According to the discussion in Remark 3, we fix $J = 3$ here. Let $\widehat{\mathcal{A}}_t = \{i : \widehat{\beta}_i(\lambda_t) \neq 0\}$ be the active set, where $\widehat{\beta}(\lambda_t)$ is the solution to the λ_t -problem. Set $\widehat{\beta}(\lambda_0) = 0$.

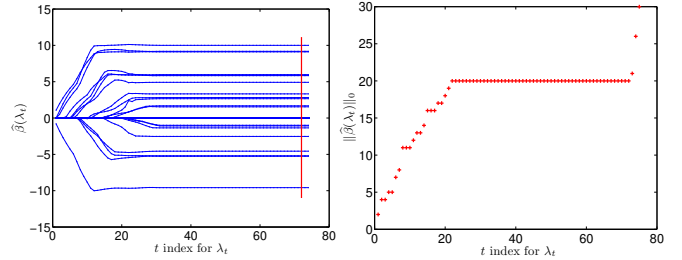


Fig. 1: The solution path of SSN with warmstarting (left panel) and the active set size along the path (right panel). The red vertical line shows the solution selected by (46).

Coupled with the warmstarting technique, Fig. 1 gives the solution path of SSN and corresponding active set size along the path, and also visualizes $\widehat{\lambda}$ and $\widehat{\beta}(\widehat{\lambda})$ (the red vertical line in the left panel) determined by the VSC selector (46). To examine the local convergence, we present in Fig. 2 the change of the active sets and the number of iterations for each fixed λ_t along the path $\lambda_0 > \lambda_1 > \dots > \widehat{\lambda}$. It is observed in Fig. 2 that $\widehat{\mathcal{A}}_t \subset \mathcal{A}$, and the size $|\widehat{\mathcal{A}}_t|$ increases monotonically as the path proceeds and eventually equals the true model size $|\mathcal{A}|$. In particular, for each λ_{t+1} problem with $\widehat{\beta}(\lambda_t)$ as the initial guess, SSN reaches convergence within one iteration in the latter part of the path, which is attributed to the local superlinear convergence of the algorithm. Hence, the overall procedure is very efficient. Fig. 3 presents the estimation error $\|\widehat{\beta}(\lambda_t) - \beta^\dagger\|$ and the prediction error (i.e., the residual) $\|X\widehat{\beta}(\lambda_t) - y\|$ along the path, as well as the underlying true β^\dagger and the solution $\widehat{\beta}(\widehat{\lambda})$ selected by (46), which demonstrates good accuracy of the algorithm.

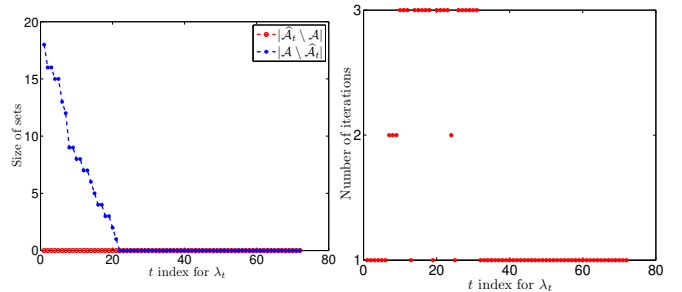


Fig. 2: The change of the active sets (left panel) and the number of iterations (left panel) for each λ_t -problem along the warmstarting path, where \mathcal{A} is the true model and $\widehat{\mathcal{A}}_t \setminus \mathcal{A}$ ($\mathcal{A} \setminus \widehat{\mathcal{A}}_t$) denotes the set difference of sets $\widehat{\mathcal{A}}_t$ and \mathcal{A} (\mathcal{A} and $\widehat{\mathcal{A}}_t$).

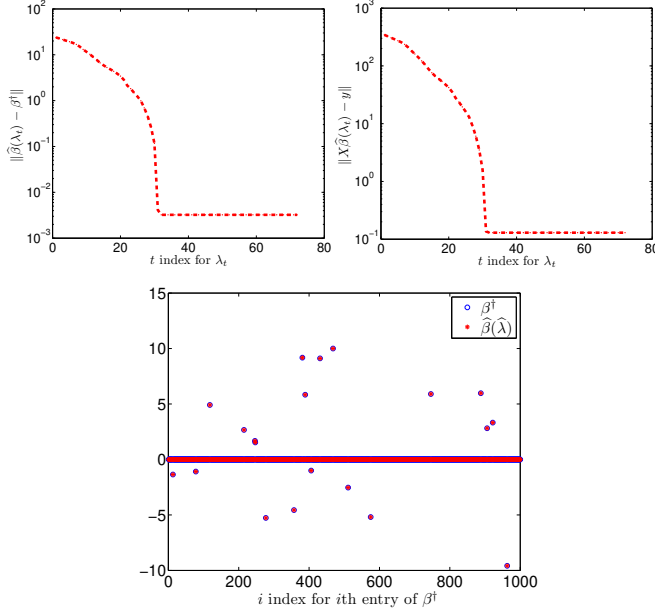


Fig. 3: The estimation error $\|\widehat{\beta}(\lambda_t) - \beta^\dagger\|$ (top left panel) and the prediction error (i.e., the residual) $\|X\widehat{\beta}(\lambda_t) - y\|$ (top right panel) along the path, and the underlying true β^\dagger and the solution $\widehat{\beta}(\widehat{\lambda})$ (bottom panel).

C. Comparison with A CD-type Algorithm

We compare our SSN algorithm with the CD algorithm in [17] for solving (5), which is summarized in Algorithm 4. The stopping criterion at step 8 of Algorithm 4 is chosen to be either $k \geq J$ or $\|\beta^{k+1} - \beta^k\| \leq \delta$ with $\delta = 1e-3$. We run CD on the same path as used in SSN with the same tuning parameter selection rule.

Algorithm 4 CD for MCP or SCAD

- 1: Input: X, y, λ, γ , initial guess β^0 and $r^0 = y - X\beta^0$. Set $k = 0$.
- 2: **for** $k = 0, 1, 2, 3, \dots$ **do**
- 3: **for** $i = 1, 2, \dots, p$ **do**
- 4: Calculate $z_i^k = X_i^T r^k + \beta_i^k$, where X_i is the i th column of X and $r^k = y - X\beta^k$ is the current residual value.
- 5: Update $\beta_i^{k+1} \leftarrow T_{\text{mcp}}(z_i^k; \lambda, \gamma)$ or $\beta_i^{k+1} \leftarrow T_{\text{scad}}(z_i^k; \lambda, \gamma)$.
- 6: Update $r^{k+1} \leftarrow r^k - (\beta_i^{k+1} - \beta_i^k)X_i$.
- 7: **end for**
- 8: Check Stop condition
If stop
Denote the last iteration by $\widehat{\beta}$.
Else
 $k := k + 1$.
- 9: **end for**
- 10: Output: $\widehat{\beta}$.

1) *Efficiency and Accuracy:* We set $p = 1000$ and 2000 with $n = \lfloor p/5 \rfloor$ and $T = \lfloor n/[2 \log(p)] \rfloor$, where $\lfloor x \rfloor$ denotes the integer part of x for $x \geq 0$. We choose three levels of

correlation $r = 0.3, 0.5$ and 0.7 , which correspond to the weak, moderate and strong correlation. We consider two levels of noise: $\sigma = 1$ (higher level) and $\sigma = 0.1$ (lower level). The number of simulations is $N = 100$.

To further illustrate the efficiency and accuracy of the proposed SSN algorithm, based on N replications, we compare it with the CD algorithm in terms of the average CPU time (Time, in seconds), the average estimated model size (MS) $N^{-1} \sum_{m=1}^N |\widehat{\mathcal{A}}^{(m)}|$, the proportion of correct models (CM, in percentage terms) $N^{-1} \sum_{m=1}^N I\{\widehat{\mathcal{A}}^{(m)} = \mathcal{A}\}$, the average ℓ_∞ absolute error (AE) $N^{-1} \sum_{m=1}^N \|\widehat{\beta}^{(m)} - \beta^\dagger\|_\infty$ and the average ℓ_2 relative error (RE) $N^{-1} \sum_{m=1}^N (\|\widehat{\beta}^{(m)} - \beta^\dagger\|_2 / \|\beta^\dagger\|_2)$. The above measures MS, CM, AE and RE evaluate the quality (accuracy) of the solutions. Clearly, the closer MS approaches to T , the closer CM approaches to 100%, and the smaller AE and RE, the higher the solution quality. Simulation results are summarized in Table I.

TABLE I: Simulation results for CD and SSN with $n = \lfloor p/5 \rfloor$ and $T = \lfloor n/[2 \log(p)] \rfloor$ based on 100 independent runs. $(M, J) = (200, 1)$.

p	r	σ	Penalty	Method	Time	MS	CM	AE	RE
1000	0.3	0.1	MCP	CD	1.3458	14.00	100%	0.0142	0.0014
				SSN	0.1920	14.00	100%	0.0183	0.0018
			SCAD	CD	1.7671	14.00	100%	0.0150	0.0015
				SSN	0.2068	14.00	100%	0.0188	0.0018
	1	0.5	MCP	CD	0.8790	14.00	100%	0.1493	0.0147
				SSN	0.1228	14.00	100%	0.1504	0.0148
			SCAD	CD	1.1659	13.90	99%	0.1778	0.0174
				SSN	0.1418	13.97	99%	0.1580	0.0152
	0.5	0.1	MCP	CD	1.3387	14.00	100%	0.0153	0.0015
				SSN	0.1849	13.78	98%	0.1489	0.0132
			SCAD	CD	1.7413	14.00	100%	0.0148	0.0015
				SSN	0.2238	14.00	100%	0.0187	0.0018
	1	0.7	MCP	CD	0.8668	13.92	98%	0.1730	0.0171
				SSN	0.1309	13.92	98%	0.1735	0.0171
			SCAD	CD	1.1434	13.82	97%	0.1809	0.0191
				SSN	0.1509	13.97	99%	0.1492	0.0147
2000	0.3	0.1	MCP	CD	1.3677	14.00	100%	0.0149	0.0015
				SSN	0.1773	13.20	90%	0.3823	0.0434
			SCAD	CD	1.7679	14.00	100%	0.0146	0.0015
				SSN	0.2168	14.00	100%	0.0190	0.0019
	1	0.5	MCP	CD	0.8786	13.95	98%	0.1787	0.0169
				SSN	0.1175	12.35	76%	0.9406	0.0983
			SCAD	CD	1.1441	13.47	91%	0.4013	0.0424
				SSN	0.1484	14.01	97%	0.1761	0.0166
	0.7	0.1	MCP	CD	3.0636	26.00	100%	0.0113	0.0011
				SSN	0.7697	26.00	100%	0.0164	0.0015
			SCAD	CD	3.8884	26.00	100%	0.0119	0.0011
				SSN	0.8128	26.00	100%	0.0169	0.0016
		1	MCP	CD	2.0280	26.00	100%	0.1165	0.0108
				SSN	0.5568	26.00	100%	0.1169	0.0108
			SCAD	CD	2.5903	26.00	100%	0.1176	0.0109
				SSN	0.5928	26.00	100%	0.1178	0.0109
	0.5	0.1	MCP	CD	3.0998	26.00	100%	0.0122	0.0010
				SSN	0.6672	26.00	100%	0.0177	0.0015
			SCAD	CD	3.9453	26.00	100%	0.0117	0.0011
				SSN	0.7062	26.00	100%	0.0168	0.0015
		1	MCP	CD	2.0312	26.00	100%	0.1204	0.0104
				SSN	0.4682	26.00	100%	0.1206	0.0105
			SCAD	CD	2.6170	26.00	100%	0.1181	0.0105
				SSN	0.5067	26.00	100%	0.1187	0.0105
	0.7	0.1	MCP	CD	3.1308	26.00	100%	0.0121	0.0011
				SSN	0.6379	24.09	84%	0.6352	0.0607
			SCAD	CD	3.9982	26.00	100%	0.0117	0.0011
				SSN	0.7078	26.00	100%	0.0178	0.0016
		1	MCP	CD	2.0787	26.00	100%	0.1189	0.0107
				SSN	0.5186	24.59	82%	0.5718	0.0561
			SCAD	CD	2.6466	25.93	97%	0.1547	0.0134
				SSN	0.5884	26.00	98%	0.1302	0.0115

For each (p, r, σ) combination, we see from Table I that SSN has better speed performance than CD for both MCP and SCAD, and SSN is about 3 ~ 9 times faster than CD. In particular, for given penalty and algorithm, CPU time decreases as σ increases, increases linearly with p , and is fairly robust to the choice of r . For SCAD, SSN and CD

are comparable in terms of solution quality. Unsurprisingly, larger σ will degrade the accuracy for both CD and SSN. When the correlation level is low or moderate (i.e., $r = 0.3$ or 0.5), similar phenomena hold for MCP. For MCP with high correlation data (i.e., $r = 0.7$), CD provides a more accurate solution than SSN does, which is due to the choice of $\gamma = 2.7$ for MCP. In fact, simulations not reported in Table I show that if we increase the value of γ for MCP, say $\gamma = 4$, SSN can also produce similar solution quality comparing with CD. Please also refer to Remark 1 for relevant discussion. Overall, the simulation results in Table I show that SSN outperforms CD in terms of CPU time while producing solutions of comparable quality.

MCP or SCAD has a free parameter γ that controls its concavity. It is important to study the sensitivity of the proposed algorithm with respect to the variation of γ . In next subsection, we conduct the sensitivity analysis for γ and other model parameters.

2) *Influence of Model Parameters*: We now consider the effects of each of the model parameters ($\gamma, n, p, r, \sigma, T$) on the performance of SSN and CD more closely in terms of the exact support recovery probability (Probability), i.e., the percentage of $\hat{\mathcal{A}}$ agrees with \mathcal{A} , and the CPU time (Time, in seconds). For the sake of simplicity, we consider γ for MCP and SCAD both, while (n, p, r, σ, T) for SCAD only, since similar variation tendency of the parameters happens for MCP. Results of Probability and Time averaged over 10 independent runs are given in Fig. 4 and Fig. 5, respectively. The parameters for solvers are set as follows.

a) *Influence of the concavity parameter γ* : Data are generated from the model with $(\gamma \in \{1.1, 2.7, 5, 10, 20\}, n = 100, p = 500, r = 0.1, \sigma = 0.1, T = 10)$ for MCP and $(\gamma \in \{2.1, 3.7, 5, 10, 20\}, n = 100, p = 500, r = 0.1, \sigma = 0.1, T = 10)$ for SCAD.

b) *Influence of the sample size n* : Data are generated from the model with $(\gamma = 3.7, n = 60 : 10 : 100, p = 500, r = 0.1, \sigma = 0.1, T = 10)$.

c) *Influence of the dimension p* : Data are generated from the model with $(\gamma = 3.7, n = 100, p = 500 : 500 : 2500, r = 0.1, \sigma = 0.1, T = 10)$.

d) *Influence of the correlation level r* : Data are generated from the model with $(\gamma = 3.7, n = 100, p = 500, r = 0.1 : 0.1 : 0.9, \sigma = 0.1, T = 10)$.

e) *Influence of the noise level σ* : Data are generated from the model with $(\gamma = 3.7, n = 100, p = 500, r = 0.1, \sigma \in \{0.2, 0.4, 0.8, 1.6, 3.2\}, T = 10)$.

f) *Influence of the sparsity level T* : Data are generated from the model with $(\gamma = 3.7, n = 100, p = 500, r = 0.1, \sigma = 0.1, T = 5 : 5 : 30)$.

In summary, the results shown in Fig. 4 and Fig. 5 demonstrate that two solvers generally have similar variation tendency with considered model parameters, and SSN is considerably faster than CD while reaching better (or comparable) accuracy, which is consistent with the simulation results in Table I. In particular, it is nice to see that the CPU time of SSN is insensitive to each of the model parameters ($\gamma, n, p, r, \sigma, T$) in Fig. 5.

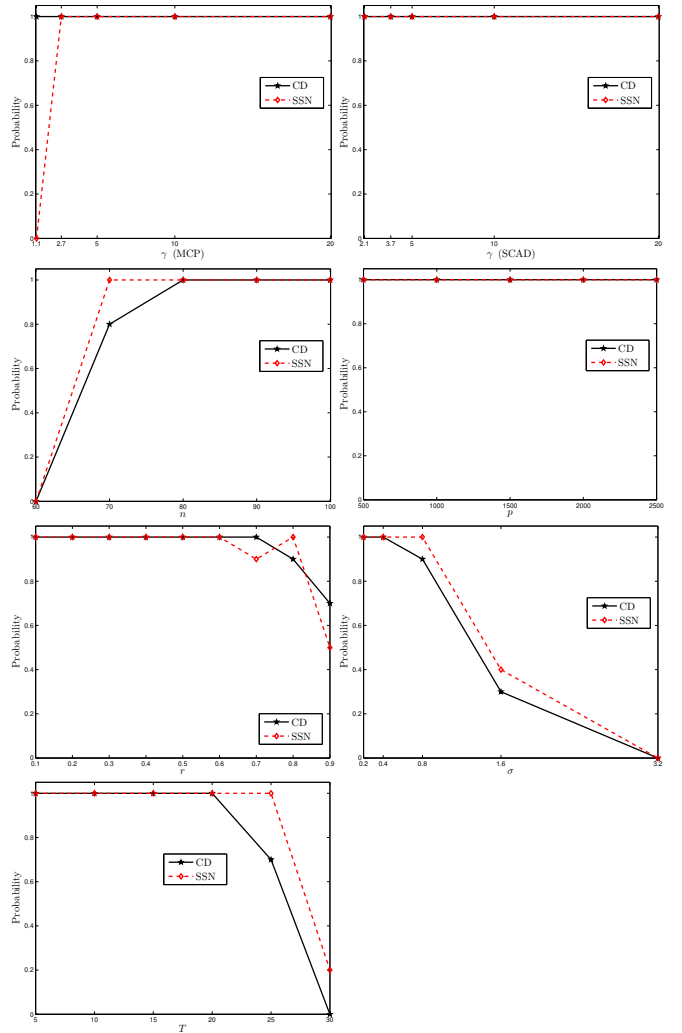


Fig. 4: Numerical results of the influence of the model parameters on the exact support recovery probability.

3) *Breast Cancer Data Example*: We analyze the breast cancer data which comes from breast cancer tissue samples deposited to The Cancer Genome Atlas (TCGA) project and compiles results obtained using Agilent mRNA expression microarrays to illustrate the application of the SSN in high-dimensional settings. This data, which is named bcTCGA, is available at <http://myweb.uiowa.edu/pbreheny/data/bcTCGA.RData>. In this bcTCGA dataset, we have expression measurements of 17814 genes from 536 patients (all expression measurements are recorded on the log scale). There are 491 genes with missing data, which we have excluded. We restrict our attention to the 17323 genes without missing values. The response variable y measures one of the 17323 genes, a numeric vector of length 536 giving expression level of gene BRCA1, which is the first gene identified that increases the risk of early onset breast cancer, and the design matrix X is a 536×17322 matrix, which represents the remaining expression measurements of 17322 genes. Because BRCA1 is likely to interact with many other genes, it is of interest to find genes with expression levels related to that of BRCA1.

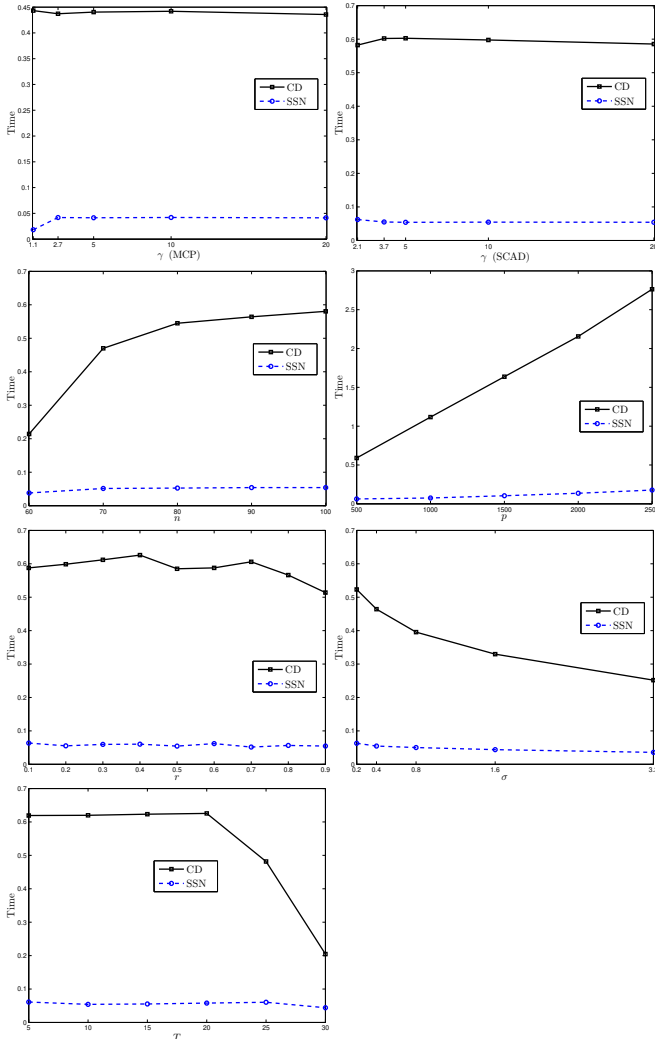


Fig. 5: Numerical results of the influence of the model parameters on the CPU time.

We consider an adaptive LASSO (ALASSO) [40] procedure using the **ncvreg** [17] and **glmnet** [41], which are R wrappers for C/Fortran, as the gold standard in comparison with SSN and CD. The following commands complete the main part of the ALASSO computation:

```

ptm <- proc.time()
library(ncvreg)
fit <- ncvreg(X, y, penalty='lasso')
beta0 <- coef(fit,which=which.min(BIC(fit)))[-1]
weight <- abs(beta0)^(-1)
weight <- pmin(weight,1e10)
library(glmnet); set.seed(0)
cvfit <- cv.glmnet(X,y,nfolds=10,penalty.factor=weight)
betahat <- coef(cvfit, s='lambda.1se')
ptm <- (proc.time()-ptm)[3]

```

We set $\gamma = 4$ and 3.7 for MCP and SCAD, respectively. Gene information, corresponding nonzero estimates, the CPU time (Time) and the prediction error (PE) are provided in Table II. From Table II, accurate to 4 decimal places, ALASSO, MCP-CD, MCP-SSN, SCAD-CD and SCAD-SSN identify 8, 5, 10, 13 and 8 genes, respectively. We observe that some genes, such as C17orf53, DTL, NBR2, SPAG5 and VPS25, are selected by at least three solvers, and in particular, all methods

capture the gene NBR2 with relatively large absolute values of the estimated coefficients. NBR2 is adjacent to BRCA1 on chromosome 17, and recent experimental evidence indicates that the two genes share a promoter [42]. It is also observed from Table II that SSN is obviously faster than ALASSO and CD while producing smaller (or comparable) PE, which demonstrates the power of SSN to identify the important biological factors from a large volume of noisy data.

TABLE II: Analysis of the bcTCGA dataset. Estimated coefficients of different methods are provided. The zero entries correspond to variables omitted.

No.	Term	Gene	MCP			SCAD	
			ALASSO	CD	SSN	CD	SSN
1	β_{1743}	C17orf53	-0.6786	-0.7361	-0.4888	-0.9269	-0.4552
2	β_{2739}	CCDC56	0	0	0.0240	0.0979	0.3883
3	β_{2964}	CDC25C	0	0	0	0.0360	0.0444
4	β_{2987}	CDC6	0	0	0	0.0089	0
5	β_{3105}	CENPK	0	0	0	0.0125	0
6	β_{4543}	DTL	0.2544	0.2883	0.2223	0.0886	0.0746
7	β_{6224}	GNL1	0	0	-0.1452	0	-0.1025
8	β_{7709}	KHDRBS1	0.1819	0	0	0	0
9	β_{7719}	KIAA0101	0	0	0	0	0.0675
10	β_{8782}	LSM12	0	0.0432	0	0	0
11	β_{9230}	MFGE8	0	0	-0.0273	0	-0.0972
12	β_{9941}	NBR2	0.4496	0.3984	0.5351	0.2408	0.5319
13	β_{11091}	PCGF1	0	0	-0.0968	0	0
14	β_{12146}	PSME3	0.1439	0	0	0.0746	0
15	β_{13518}	SETMAR	0	0	-0.0807	0	0
16	β_{14296}	SPAG5	0.0035	0.0598	0.2370	0.0117	0.0688
17	β_{14397}	SPRY2	0	0	0	-0.0058	0
18	β_{15122}	TIMELESS	0	0	0	0.0322	0
19	β_{15535}	TOP2A	0	0	0	0.0299	0
20	β_{15882}	TUBA1B	0.0857	0	0	0	0
21	β_{16315}	VPS25	0.2560	0.2372	0.3581	0.0998	0
22	β_{16640}	ZBTB26	0	0	-0.1015	0	0
Time			14.7600	28.7712	3.3998	30.8354	3.1835
PE			0.2116	0.2344	0.1837	0.2639	0.2117

To further evaluate the performance of SSN relative to CD on the quality of variable selection, we conduct the cross-validation procedure similar to [43], [44]. We conduct 50 random partitions of the data. For each partition, we randomly choose $3/4$ observations and $1/4$ observations as the training and test data, respectively. We compute the CPU time (Time, in seconds) and the model size (MS, i.e., the number of selected genes) using the training data, and calculate the prediction error (PE) based on the test data. Table III presents the average values over 50 random partitions, along with corresponding standard deviations in the parentheses. As shown in Table III, SSN performs quite better than CD in terms of the CPU time while producing comparable PE. Based on 50 random partitions, we also report the selected genes and their corresponding frequency (Freq) in Table IV, where the genes are ordered such that the frequency is decreasing. To save space, we only list genes with frequency greater than or equal to 5 counts. For each scenario, it is observed from Table IV that the gene NBR2 is the top 1 gene ranked according to the frequency and has a significantly higher frequency than other genes, which is consistent with the findings of Table II and [42], and largely implies this gene is most closely related to BRCA1.

D. Comparison with the DCPN

As the supplement of Section III-D, we conduct numerical experiments to compare the DCPN and SSN. The implementation setting and comparison metrics are given from Section IV-A and IV-C, respectively. The noise level $\sigma = 1$ is fixed.

TABLE III: The CPU time (Time), model size (MS) and prediction error (PE) averaged across 50 random partitions of the real data (numbers in parentheses are standard deviations)

Penalty	Method	Time	MS	PE
MCP	CD	25.3317(1.4440)	7.02(2.8820)	0.2761(0.0451)
	SSN	2.5452(0.4913)	9.46(3.7591)	0.2914(0.0568)
SCAD	CD	26.0625(1.4431)	9.46(3.3025)	0.3190(0.0624)
	SSN	2.5736(0.4382)	9.00(4.4584)	0.2647(0.0471)

TABLE IV: Frequency table for 50 random partitions of the real data. To save space, only the genes with $\text{Freq} \geq 5$ are listed.

MCP		SCAD	
CD	SSN	CD	SSN
Gene	Freq	Gene	Freq
NBR2	50	NBR2	46
DTL	36	C17orf53	40
VPS25	31	MFGE8	11
C17orf53	25	VPS25	10
CCDC56	12	GNL1	10
CDC25C	12	PSME3	8
SPAG5	12	C3orf10	8
PSME3	12	DTL	7
LSM12	11	TIMELESS	7
TOP2A	8	CDC25C	20
KLHL13	8	CENPK	15
SPRY2	8	SPAG5	14
NPR2	7	CCDC43	12
TUBA1B	7	MCM6	6
TIMELESS	6	CDC6	12
KIAA0101	6	SETMAR	6
CENPK	5	FBXO18	6
CRBN	5	RDM1	8
VDAC1	5	SPRY2	9
CMTM5	5	KLHL13	6
CDC6	5	AASDH	5
		YTHDC2	5
		DYNLL1	5
		TUBG1	5
		HMGN2	5
		CENPQ	5
		CRBN	5
		C10orf30	5

The DCPN is implemented using the picasso package [37], [45]. For both solvers, we use the HBIC selector to choose proper tuning parameters. We set $\gamma = 4$ and 3.7 for MCP and SCAD, respectively. Simulation results are summarized in Table V.

TABLE V: Simulation results for DCPN and SSN with $n = \lfloor p/5 \rfloor$ and $T = \lfloor n/[2 \log(p)] \rfloor$ based on 10 independent runs. $(M, J) = (100, 1)$ and $\sigma = 1$.

p	r	Penalty	Method	Time	MS	CM	AE	RE
1000	0.3	MCP	DCPN	0.147	14.0	100%	0.9821	0.0620
			SSN	0.057	14.0	100%	0.1456	0.0142
		SCAD	DCPN	0.145	14.0	100%	0.9870	0.0654
	0.7	MCP	DCPN	0.059	14.0	100%	0.1456	0.0142
			SSN	0.045	11.9	80%	1.3921	0.1255
		SCAD	DCPN	0.154	15.0	0%	0.5866	0.0467
2000	0.3	MCP	DCPN	0.059	14.0	100%	0.1693	0.0149
			SSN	0.209	26.0	100%	0.1210	0.0104
		SCAD	DCPN	0.248	26.0	100%	0.1436	0.0715
	0.7	MCP	DCPN	0.222	26.0	100%	0.1210	0.0104
			SSN	0.200	23.5	90%	0.9125	0.0998
		SCAD	DCPN	0.262	26.9	10%	0.6178	0.0546
		SSN	0.222	26.0	100%	0.1172	0.0108	

For each combination, it is observed from Table V that SSN has better speed performance than DCPN by Time. Further, considering that the SSN is written in pure Matlab while the picasso is a R wrapped C solver, it is fair to say that the proposed SSN is a highly efficient method for solving the problem (5). In addition, the CPU time generally increases linearly with p , and is relatively robust to the choice of r .

When the correlation is low (i.e., $r = 0.3$), both solvers can select the true model 100 percent correctly, while SSN can produce solutions with smaller AE and RE comparing with DCPN. In high correlation level (i.e., $r = 0.7$), the SSN still behaves well in terms of CM, while the DCPN almost fails on this metric, and both solvers share comparable AE and RE. In summary, the results in Table V show good performance of SSN in terms of both efficiency and accuracy.

V. CONCLUSION

Starting from the KKT condition we developed Semi-smooth Newton (SSN) algorithm for the MCP and SCAD regularized linear regression problem in high dimensional settings. We established the local superlinear convergence of SSN and analyzed its computational complexity. Combining the VSC or HBIC tuning parameter selector with warm start, we obtain the solution path and select the tuning parameters in a fast and stable way. Numerical comparisons with the CD and the DCPN are presented to demonstrate the efficiency and accuracy of the SSN. We make all these innovations publicly available by developing a Matlab package named *ssn-nonconvex* available at <http://faculty.zuel.edu.cn/tjyjxxy/jyl/list.htm>.

We will generalize SSN to group MCP/ SCAD or to regression problems with other loss functions in our future work. Semi-smooth Newton methods converges superlinearly but locally, we adopt simple continuation strategy to globalize it. Globalization via smoothing Newton methods [46], [47], [48] is also of immense interest.

APPENDIX

A. Proof of Lemma 1

Proof: See [17] and [18]. \blacksquare

B. Proof of Theorem 1

Proof: Here we give the proof for the results for MCP since the proof for SCAD penalty is similar. Let $\hat{\beta} \in \mathbb{R}^p$ be a global minimizer of

$$E_{mcp}(\beta) := \frac{1}{2} \|X\beta - y\|_2^2 + \sum_{i=1}^p p_{mcp}(\beta_i; \lambda, \gamma).$$

Define

$$f_i(t) = E_{mcp}(\hat{\beta}_1, \dots, \hat{\beta}_{i-1}, t, \hat{\beta}_{i+1}, \dots, \hat{\beta}_p), i = 1, 2, \dots, p.$$

Then, by definition $\hat{\beta}_i$ is a global minimizer of the scalar function $f_i(t)$. Some algebra shows that the minimizer of $f_i(t)$ is also the minimizer of $\frac{1}{2}(t - (\hat{\beta}_i + X_i^T(y - X\hat{\beta})))^2 + p_{mcp}(t; \lambda, \gamma)$. Then $\hat{\beta}_i = T_{mcp}(\hat{\beta}_i + X_i^T(y - X\hat{\beta}); \lambda, \gamma)$ by Lemma 1. (15) - (16) follow from the definition of $G = X^T X$, $\tilde{y} = X^T y$ and $\mathbb{T}(\cdot; \lambda, \gamma)$.

Conversely, assume that $(\hat{\beta}, \hat{d})$ satisfying (15) - (16). Then $\forall i, \hat{\beta}_i = T_{mcp}(\hat{\beta}_i + X_i^T(y - X\hat{\beta}); \lambda, \gamma)$ which implies that $\hat{\beta}_i$ is a minimizer of the $f_i(t)$ defined above. This shows $\hat{\beta}$ is a coordinate-wise minimizer of E_{mcp} . By Lemma 3.1 in [49], $\hat{\beta}$ is also a stationary point. \blacksquare

C. Proof of Lemma 2

Proof: Observing that both $T_{scad}(\cdot; \lambda, \gamma)$ and $T_{mcp}(\cdot; \lambda, \gamma)$ are piecewise linear function on \mathbb{R}^1 , it suffices to prove that the piecewise linear scalar function

$$f(t) = \begin{cases} k_1 t + b_1, & \text{if } t \leq t_0, \\ k_2 t + b_2, & \text{if } t > t_0. \end{cases}$$

is Newton differentiable with

$$\nabla_N f(t) = \begin{cases} k_1, & t < t_0, \\ r \in \mathbb{R}^1, & t = t_0, \\ k_2, & t_0 < t. \end{cases} \quad (49)$$

where k_1, k_2, b_1, b_2, t_0 are arbitrary such that $k_1 t_0 + b_1 = k_2 t_0 + b_2$. Indeed, let

$$D(t+h)h = \begin{cases} k_1 h, & t < t_0, \\ k_2 h, & t_0 < t, \end{cases}$$

and $G(t_0)h = rh$ with an arbitrary $r \in \mathbb{R}$, then $|f(t+h) - f(t) - D(t+h)h|/|h| \rightarrow 0$ as $|h| \rightarrow 0$. \blacksquare

D. Proof of Theorem 2

Proof: Here we give the proof for the results for MCP since the proof for SCAD penalty is similar. Let

$$b(t; \lambda, \gamma) = \begin{cases} 0, & |t| \leq \lambda, \\ 1/(1-1/\gamma), & \lambda < |t| < \gamma\lambda, \\ 1, & \gamma\lambda \geq |t|, \end{cases} \quad \mathbf{b}(x; \lambda, \gamma) =$$

$\text{diag}[b(x_1; \lambda, \gamma), \dots, b(x_p; \lambda, \gamma)]'$, $g_i(x) = T_{mcp}(e_i^T x; \lambda, \gamma) : x \in \mathbb{R}^p \rightarrow \mathbb{R}^1, i = 1, \dots, p$, where the column vector e_i is the i th orthonormal basis in \mathbb{R}^p , $\mathbb{T}(x; \lambda, \gamma) = [g_1(x), \dots, g_p(x)]'$. It follows Lemma 2 and (9)-(11) that $b(t; \lambda, \gamma) \in \nabla_N T_{mcp}(t)$ and

$$\mathbf{b}(x; \lambda, \gamma) \in \nabla_N \mathbb{T}(x; \lambda, \gamma). \quad (50)$$

Then, by (50) and (9)-(11) the vector value function $F_1(\beta; d)$ is Newton differentiable and

$$[H_{11}^k \quad H_{12}^k] \in \nabla_N F_1(z_{mcp}^k), \quad (51)$$

where H_{11}^k, H_{12}^k are in the form of (25). By (9)-(11), $F_2(\beta; d)$ is Newton differentiable and

$$[H_{21}^k \quad H_{22}^k] \in \nabla_N F_2(z_{mcp}^k), \quad (52)$$

where H_{21}^k, H_{22}^k are in the form of (25). It follows (51)-(52) and (9)-(11) that $H_{mcp}^k \in \nabla_N F_{mcp}(z_{mcp}^k)$.

The uniform boundedness of $(H_{mcp}^k)^{-1}$ is derived similarly as the proof of Theorem 2.6 in [44]. \blacksquare

E. Proof of Theorem 3

Proof: Here we give the proof for the results for MCP since the proof for SCAD penalty is similar. Let z_{mcp}^k be sufficiently close to z_{mcp}^* which is a root of F_{mcp} . By the definition of Newton derivative we have,

$$\begin{aligned} & \|H_{mcp}^k(z_{mcp}^k - z_{mcp}^*) - F_{mcp}(z_{mcp}^k) + F_{mcp}(z_{mcp}^*)\|_2 \\ & \leq \epsilon \|z_{mcp}^k - z_{mcp}^*\|_2, \end{aligned} \quad (53)$$

where $\epsilon \rightarrow 0$ as $z_{mcp}^k \rightarrow z_{mcp}^*$. Then, by the definition of SSN and the fact $F_{mcp}(z_{mcp}^*) = 0$ we get

$$\|z_{mcp}^{k+1} - z_{mcp}^*\|_2$$

$$\begin{aligned} & = \|z_{mcp}^k - (H_{mcp}^k)^{-1} F_{mcp}(z_{mcp}^k) - z_{mcp}^*\|_2 \\ & = \|z_{mcp}^k - (H_{mcp}^k)^{-1} F_{mcp}(z_{mcp}^k) - z_{mcp}^* + (H_{mcp}^k)^{-1} F_{mcp}(z_{mcp}^*)\|_2 \\ & \leq \|(H_{mcp}^k)^{-1}\| \|H_{mcp}^k(z_{mcp}^k - z_{mcp}^*) - F_{mcp}(z_{mcp}^k) + F_{mcp}(z_{mcp}^*)\|_2 \\ & \leq M_\gamma \epsilon \|z_{mcp}^k - z_{mcp}^*\|_2. \end{aligned}$$

The last inequality follows from (53) and the uniform boundedness of $(H_{mcp}^k)^{-1}$ proved in Theorem 2. Then the sequence z_{mcp}^k generated by Algorithm 2 converges to z_{mcp}^* locally and superlinearly. \blacksquare

ACKNOWLEDGMENT

The authors are grateful to the editor, the associate editor and three anonymous referees for their many constructive and insightful comments that have led to significant improvements in the article. The authors also would like to thank Professor Defeng Sun for the helpful discussion on the algorithm.

REFERENCES

- [1] B. K. Natarajan, "Sparse approximate solutions to linear systems," *SIAM Journal on Computing*, vol. 24, no. 2, pp. 227–234, 1995.
- [2] R. Tibshirani, "Regression shrinkage and selection via the lasso," *Journal of the Royal Statistical Society. Series B (Methodological)*, vol. 58, no. 1, pp. 267–288, 1996.
- [3] S. S. Chen, D. L. Donoho, and M. A. Saunders, "Atomic decomposition by basis pursuit," *SIAM Review*, vol. 43, no. 1, pp. 129–159, 2001.
- [4] M. R. Osborne, B. Presnell, and B. A. Turlach, "A new approach to variable selection in least squares problems," *IMA Journal of Numerical Analysis*, vol. 20, no. 3, pp. 389–403, 2000.
- [5] B. Efron, T. Hastie, I. Johnstone, and R. Tibshirani, "Least angle regression," *The Annals of Statistics*, vol. 32, no. 2, pp. 407–499, 2004.
- [6] W. J. Fu, "Penalized regressions: the bridge versus the lasso," *Journal of Computational and Graphical Statistics*, vol. 7, no. 3, pp. 397–416, 1998.
- [7] J. Friedman, T. Hastie, H. Höfling, and R. Tibshirani, "Pathwise coordinate optimization," *The Annals of Applied Statistics*, vol. 1, no. 2, pp. 302–332, 2007.
- [8] T. T. Wu and K. Lange, "Coordinate descent algorithms for lasso penalized regression," *The Annals of Applied Statistics*, vol. 2, no. 1, pp. 224–244, 2008.
- [9] E. J. Candes and T. Tao, "Decoding by linear programming," *IEEE Transactions on Information Theory*, vol. 51, no. 12, pp. 4203–4215, 2005.
- [10] N. Meinshausen and P. Bühlmann, "High-dimensional graphs and variable selection with the lasso," *The Annals of Statistics*, vol. 34, no. 3, pp. 1436–1462, 2006.
- [11] P. Zhao and B. Yu, "On model selection consistency of lasso," *Journal of Machine Learning Research*, vol. 7, no. Nov, pp. 2541–2563, 2006.
- [12] J. Fan and R. Li, "Variable selection via nonconcave penalized likelihood and its oracle properties," *Journal of the American Statistical Association*, vol. 96, no. 456, pp. 1348–1360, 2001.
- [13] C.-H. Zhang, "Nearly unbiased variable selection under minimax concave penalty," *The Annals of Statistics*, vol. 38, no. 2, pp. 894–942, 2010.
- [14] K. Lange, D. R. Hunter, and I. Yang, "Optimization transfer using surrogate objective functions (with discussion)," *Journal of Computational and Graphical Statistics*, vol. 9, no. 1, pp. 1–59, 2000.
- [15] T. Zhang, "Analysis of multi-stage convex relaxation for sparse regularization," *Journal of Machine Learning Research*, vol. 11, no. Mar, pp. 1081–1107, 2010.
- [16] H. Zou and R. Li, "One-step sparse estimates in nonconcave penalized likelihood models," *The Annals of Statistics*, vol. 36, no. 4, pp. 1509–1533, 2008.
- [17] P. Breheny and J. Huang, "Coordinate descent algorithms for nonconvex penalized regression, with applications to biological feature selection," *The Annals of Applied Statistics*, vol. 5, no. 1, p. 232, 2011.
- [18] R. Mazumder, J. H. Friedman, and T. Hastie, "Sparsenet: Coordinate descent with nonconvex penalties," *Journal of the American Statistical Association*, vol. 106, no. 495, pp. 1125–1138, 2011.

[19] G. Li and T. K. Pong, "Calculus of the exponent of kurdyka-lojasiewicz inequality and its applications to linear convergence of first-order methods," *Found Comput Math, In press*, <https://doi.org/10.1007/s10208-017-9366-8>, 2017.

[20] B. Kummer, "Newton's method for non-differentiable functions," *Advances in mathematical optimization*, vol. 45, pp. 114–125, 1988.

[21] L. Qi and J. Sun, "A nonsmooth version of newton's method," *Mathematical programming*, vol. 58, no. 1-3, pp. 353–367, 1993.

[22] K. Ito and K. Kunisch, *Lagrange multiplier approach to variational problems and applications*. SIAM, 2008.

[23] X. Chen, Z. Nashed, and L. Qi, "Smoothing methods and semismooth methods for nondifferentiable operator equations," *SIAM Journal on Numerical Analysis*, vol. 38, no. 4, pp. 1200–1216, 2000.

[24] D. L. Donoho and I. M. Johnstone, "Adapting to unknown smoothness via wavelet shrinkage," *Journal of the American Statistical Association*, vol. 90, no. 432, pp. 1200–1224, 1995.

[25] C.-H. Zhang and J. Huang, "The sparsity and bias of the lasso selection in high-dimensional linear regression," *The Annals of Statistics*, vol. 36, no. 4, pp. 1567–1594, 2008.

[26] Y. She, "Thresholding-based iterative selection procedures for model selection and shrinkage," *Electronic Journal of Statistics*, vol. 3, pp. 384–415, 2009.

[27] A. Beck and M. Teboulle, "A fast iterative shrinkage-thresholding algorithm for linear inverse problems," *SIAM Journal on Imaging Sciences*, vol. 2, no. 1, pp. 183–202, 2009.

[28] Y. Jiao, B. Jin, and X. Lu, "A primal dual active set with continuation algorithm for the ℓ^0 -regularized optimization problem," *Applied and Computational Harmonic Analysis*, vol. 39, no. 3, pp. 400–426, 2015.

[29] Q. Fan, Y. Jiao, and X. Lu, "A primal dual active set algorithm with continuation for compressed sensing," *IEEE Transactions on Signal Processing*, vol. 62, no. 23, pp. 6276–6285, 2014.

[30] Y. Jiao, B. Jin, and X. Lu, "Group sparse recovery via the $\ell^0(\ell^2)$ penalty: theory and algorithm," *IEEE Transactions on Signal Processing*, vol. 65, no. 4, pp. 998–1012, 2017.

[31] Y. Shi, Y. Wu, D. Xu, and Y. Jiao, "An ADMM with continuation algorithm for non-convex SICA-penalized regression in high dimensions," *Journal of Statistical Computation and Simulation*, vol. 88, no. 9, pp. 1826–1846, 2018.

[32] J. Huang, Y. Jiao, X. Lu, and L. Zhu, "Robust decoding from 1-bit compressive sampling with least squares," *SIAM Journal on Scientific Computing*, vol. 40, no. 4, pp. A2062–A2086, 2018.

[33] L. Wang, Y. Kim, and R. Li, "Calibrating nonconvex penalized regression in ultra-high dimension," *The Annals of Statistics*, vol. 41, no. 5, pp. 2505–2536, 2013.

[34] Y. Shi, Y. Jiao, Y. Cao, and Y. Liu, "An alternating direction method of multipliers for mcp-penalized regression with high-dimensional data," *Acta Mathematica Sinica, English Series*, vol. <https://doi.org/10.1007/s10114-018-7096-8>, 2018.

[35] J. Huang, Y. Jiao, B. Jin, J. Liu, X. Lu, and C. Yang, "A unified primal dual active set algorithm for nonconvex sparse recovery," *arXiv preprint arXiv:1310.1147v4*, 2018.

[36] X. Li, L. Yang, J. Ge, J. Haupt, T. Zhang, and T. Zhao, "On quadratic convergence of dc proximal newton algorithm in nonconvex sparse learning," in *Advances in Neural Information Processing Systems*, 2017, pp. 2742–2752.

[37] T. Zhao, H. Liu, T. Zhang *et al.*, "Pathwise coordinate optimization for sparse learning: Algorithm and theory," *The Annals of Statistics*, vol. 46, no. 1, pp. 180–218, 2018.

[38] A. F. Izzailov and M. V. Solodov, *Newton-type methods for optimization and variational problems*. Springer, 2014.

[39] S. Becker, J. Bobin, and E. J. Candès, "Nesta: A fast and accurate first-order method for sparse recovery," *SIAM Journal on Imaging Sciences*, vol. 4, no. 1, pp. 1–39, 2011.

[40] H. Zou, "The adaptive lasso and its oracle properties," *Journal of the American Statistical Association*, vol. 101, no. 476, pp. 1418–1429, 2006.

[41] J. Friedman, T. Hastie, and R. Tibshirani, "Regularization paths for generalized linear models via coordinate descent," *Journal of Statistical Software*, vol. 33, no. 1, pp. 1–22, 2010.

[42] P. Breheny, "Marginal false discovery rates for penalized regression models," *arXiv preprint arXiv:1607.05636v2*, 2017.

[43] J. Huang, S. Ma, and C.-H. Zhang, "Adaptive lasso for sparse high-dimensional regression models," *Statistica Sinica*, vol. 18, pp. 1603–1618, 2008.

[44] C. Yi and J. Huang, "Semismooth newton coordinate descent algorithm for elastic-net penalized huber loss regression and quantile regression," *Journal of Computational and Graphical Statistics*, vol. 26, no. 3, pp. 547–557, 2017.

[45] J. Ge, X. Li, H. Jiang, H. Liu, T. Zhang, M. Wang, and T. Zhao, *Picasso: A sparse learning library for high dimensional data analysis in R and Python*, 2017, version 1.2.0. [Online]. Available: <https://CRAN.R-project.org/package=picasso>

[46] X. Chen, L. Qi, and D. Sun, "Global and superlinear convergence of the smoothing newton method and its application to general box constrained variational inequalities," *Mathematics of Computation of the American Mathematical Society*, vol. 67, no. 222, pp. 519–540, 1998.

[47] L. Qi and D. Sun, "A survey of some nonsmooth equations and smoothing newton methods," in *Progress in optimization*. Springer, 1999, pp. 121–146.

[48] L. Qi, D. Sun, and G. Zhou, "A new look at smoothing newton methods for nonlinear complementarity problems and box constrained variational inequalities," *Mathematical programming*, vol. 87, no. 1, pp. 1–35, 2000.

[49] P. Tseng, "Convergence of a block coordinate descent method for nondifferentiable minimization," *Journal of Optimization Theory and Applications*, vol. 109, no. 3, pp. 475–494, 2001.